Dilatometric study of continuous annealing of a cold-rolled austenitic stainless steel

Abdelali Hayoune, Halima Maredj, Jamal Fajoui, Pierre-Antoine Dubos

Dilatometric study of continuous annealing of a cold-rolled austenitic stainless steel

Abdelali Hayoune[a,b,*], Halima Maredj[c], Jamal Fajoui[d], Pierre-Antoine Dubos[d,*].

[a] Laboratoire de Technologie des Matériaux Avancés, Ecole Nationale Polytechnique de Constantine, BP 75A RP Ali Mendjeli, Constantine, Algérie.
[b] Laboratoire de Transformations de Phases, Université des Frères Mentouri - Constantine 1, Route d'Ain El bey, Constantine, Algérie.
[c] Plateforme Technologique, Ecole Nationale Polytechnique de Constantine, BP 75A RP Ali Mendjeli, Constantine, Algérie.
[d] Nantes Université, Ecole Centrale Nantes, CNRS, GeM, UMR 6183, F-44600 Saint-Nazaire, France.

[*]Corresponding authors: athayoune@yahoo.fr, pierre-antoine.dubos@univ-nantes.fr

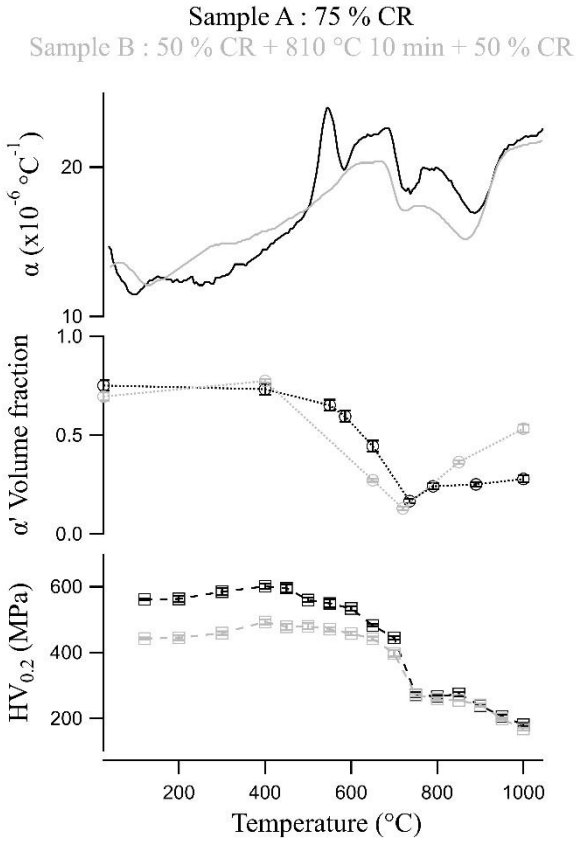

Graphical abstract: Influence of the CR strategy on dilatometric behavior, microstructure and hardness.

Abstract:

The sequence of structural changes produced in two deformed microstructures of austenitic stainless steel (ASS) elaborated by a multi-pass unidirectional cold rolling (CR) and a two-step one, to a 75 % thickness reduction, was followed by dilatometric experiments. The two materials showed different dilatometric behaviors. XRD and microhardness measurements were performed to underly the observed dilatometric behaviors. The material subjected to multi-pass unidirectional CR showed an unusual dilatometric behavior. The first heating stage led to the occurrence of the recovery reaction in competition with the ε-martensite reversion. When the temperature increased between 550 and 780 °C, the reversion of deformation induced α-martensite took place and led to a complicated dilatometric anomaly. Further increase in temperature led to the occurrence of the recrystallization transformation. However, the material subjected to two-step CR showed a quite usual dilatometric behavior which was explained by the occurrence of several reactions in the following order: (i) T < 300 °C, the recovery reaction, (ii) 300 < T < 680 °C, the ferro

to paramagnetic transformation of α-martensite, the reversion of ε-martensite and the athermal reversion of α-martensite, (iii) 680 < T <760 °C, thermal reversion of DIM and then (iv) at T > 760 °C, the recrystallization.

1. Introduction

The mechanical behavior of metallic materials is essentially determined by the nature and density of dislocations, and their ability to move. The strengthening of these materials is increased by restricting dislocation motion due to the presence of various types of obstacles such as other dislocations, grains, subgrains, or cell boundaries (grain refinement), solute atoms, and second-phase particles, either alone or in combination [1-3].

Owing to a good combination of excellent ductility, toughness, and corrosion resistance, commercial austenitic stainless steels (ASSs) have been widely used as structural materials for various engineering applications [4-9]. However, they exhibit quite low yield strength derived from the coarse γ-austenite (face-centered cubic (FCC)) phase [9-12]. According to several studies conducted in this research area, the yield strengthening of ASSs can be reached through severe plastic deformation (SPD) methods [6, 11-13] via the activation of various strengthening mechanisms, such as grain refining, transformation strengthening and work hardening. However, these methods are very limited by the fact that mass production of high strength materials is very difficult [6, 11, 13]. Therefore, conventional metalworking techniques, where one or more dimensions of the work piece are continuously reduced under processing, can be used instead of complicated SPD methods [12, 13]. Furthermore, it has also been reported that ultrafine grained (UFG) ASSs can be fabricated by conventional rolling and annealing processes [4 - 7, 9, 11 - 17]. The principle is to use CR to produce DIM and the subsequent annealing to revert the DIM back to nano- or ultrafine-grained austenite under specific conditions [4 - 6, 9, 12 -15, 17]. Additionally, the ultrafine or fine-grained strengthening is a hopeful pathway to improve simultaneously the yield strength, toughness and corrosion resistance of ASSs without obviously deteriorating ductility and work-hardening ability [12].

It has been demonstrated that during the early stages of low temperature deformation of ASSs, ε (Hexagonal Close Packed (HCP), non-ferromagnetic) martensite forms at shear bands and stacking faults (SF) whereasα’ (Body Centered Cubic BCC, ferromagnetic) martensite nucleates at the intersections of the shear bands [4, 9, 10, 17 - 19]. By increasing the deformation level, α’-martensite grows by consuming ε-

martensite and austenite phases [4, 9, 10, 17 - 19]. The amount of created martensite depends on processing parameters such as temperature, deformation rate and steel composition as well [4, 6, 10 - 13, 16, 17, 18, 20]. During the subsequent annealing, the formed martensite plates provide a high density of nucleation sites to reverse austenite formation, which, gives rise to UFG microstructure under specific conditions of the annealing treatment, [4 - 6, 9, 12, 13, 15, 17, 21].

During the reversion transformation of DIM α', recovery and recrystallization may occur simultaneously or sequentially, and the obtained microstructure shows bimodal or multimodal distribution of grain sizes [4, 6, 7, 9, 12, 13, 15, 17, 21]. Hence, the efficiency of the grain refinement treatment can be improved by understanding the different transformations occurring during the annealing treatment.

The present work mainly focuses on the evolution of the microstructure, through a continuous annealing of an ASS prepared by cold rolling following two different paths: (i) a severe plastic deformation by rolling at room temperature up to a thickness reduction rate of 75 % and (ii) a two-step cold rolling thermomechanical treatment composed of: CR up to 50 %, annealing at 810 °C for 10 min and a second CR up to 50 % (leading to a total thickness reduction rate of 75 %). The objective of the intermediate annealing treatment carried out at 810 °C is to get a partial reversion of the DIM and to recrystallize the deformed microstructure and hence, a primary grain refinement of the as-received sample.

2. Experimental procedure

The experimental material was a Fe-Ni-Cr low carbon ASS with an alloy composition (wt. pct.) mentioned in **Table 1**. The as-received plate having 8 mm in thickness was used as the starting material.

Table 1. Chemical Composition of the investigated Stainless Steel (Mass Percent)

C	Ni	Cr	Si	Mn	Cu	Co	Fe
0.053	14,8	9	0.3	1.65	0.2	0.15	Bal

Several specimens with the size of 5×3 cm^2 were cut from the plates for CR. The CR was carried out in a two-high rolling mill. The first type of samples (Sample A) was obtained by multi-pass unidirectional CR to a 75 % thickness reduction while the second one (Sample B) was obtained by a two-step CR. In the first step, the material was cold-rolled to a 50 % thickness reduction and then annealed at 810 °C for 10 min.

After that, the sample was cold-rolled to 50 % thickness reduction to gain a total thickness reduction of 75 %.

The thermal expansion of the studied samples was analyzed with a Netzsch dilatometer (DIL402 C). Specimens, taken from the Rolling Direction (RD) and having dimensions of 20 x 2 x 4 mm^3, were placed in contact with the pushrod and heated up to 1050 °C, under an argon gas flow of 100 ml /min and a heating rate of 5 °C/min. In order to avoid dilatometric artifacts, a dilatometric test was repeated twice and the presented dilatometric curves were obtained after the subtraction of a correction curve obtained by measuring the dilatation of a calibration standard (Al_2O_3) under the same conditions as the measured sample.

The microstructural observation was carried out by an Optical Microscope (OM) using Oxion - Euromex and Scanning Electron Microscopy (SEM) on a Jeol 7100 field-emission SEM.

The phase analyses were carried out by using X-ray diffraction (XRD) on an Empyrean, Malvern Panalytical diffractometer, equipped with Cu K_α radiation. The XRD patterns were recorded in θ–θ scanning mode with a step width of 0.053° and a counting time of 40 s using 1D fast detector (Pixel). The XRD measurements were carried out in RD-TD plane and specimens were electro-polished to remove DIM from the surface.

Specimens for microstructural analysis were prepared by a careful mechanical polishing so as to avoid DIM formation followed by electro-polishing using the Lectropol - 5 (Struers) electrolytic-polishing machine and the A2 solution.

The BCC phase volume fraction (denoted f_{BCC}) was determined, for each measurement point, using the equation (1), as formulated by Bonarski *et al*. [22] and used in previous works [23, 24]:

$$f^{BCC} = \left(1 + \frac{I_{hkl}^{FCC}}{I_{hkl}^{BCC}} \frac{R_{hkl}^{BCC}}{R_{hkl}^{HCP}}\right)^{-1} \quad (1)$$

where I_{hkl} is the integrated intensity of the corresponding {hkl} peak and R_{hkl} is the reflectivity of the lattice plane {hkl}, given by the following equation (2) [22]:

$$R_{hkl} = \frac{1}{v^2} |F_{hkl}|^2 \left(\frac{1 + \cos^2(2\theta)}{\sin^2(2\theta)\cos(\theta)}\right) m \frac{e^{-2M}}{\mu} \quad (2)$$

where V is the volume of the unit cell (in $Å^3$), F_{hkl} is the structure factor, 2θ is the considered Bragg angle (in rad), m is the {hkl} planes multiplicity factor, μ is the linear absorption coefficient (in cm^{-1}) and e^{-2M} is the Debye-Waller factor.

The volume fraction of each phase was calculated from several groups of family planes, as presented in **Table 2**, in order to obtain the average BCC phase distribution and evaluate the influence of the texture on the quantitative phase analysis.

Table 2. Groups of family planes used to obtain the average BCC phase distribution.

Planes family couples	$\{111\}_{FCC}/\{110\}_{BCC}$
	$\{111\}_{FCC}/\{200\}_{BCC}$
	$\{111\}_{FCC}/\{211\}_{BCC}$
	$\{200\}_{FCC}/\{110\}_{BCC}$
	$\{200\}_{FCC}/\{200\}_{BCC}$
	$\{200\}_{FCC}/\{211\}_{BCC}$
	$\{220\}_{FCC}/\{110\}_{BCC}$
	$\{220\}_{FCC}/\{200\}_{BCC}$
	$\{220\}_{FCC}/\{211\}_{BCC}$
	$\{311\}_{FCC}/\{110\}_{BCC}$
	$\{311\}_{FCC}/\{200\}_{BCC}$
	$\{311\}_{FCC}/\{211\}_{BCC}$

The evolution of the mechanical properties of the studied samples (as a function of temperature), was followed by Vickers micro-hardness measurements, by means of a Vickers micro-hardness tester INNOVATEST with a diamond pyramid indenter and an applied load of 200 g and dwell time of 10 s.

3. Results and discussion

3.1. Microstructural analysis

The microstructure of the as-received sample is shown in **Fig. 1**. The microstructure is composed of equiaxed grains having an average size in the order of 11 μm.

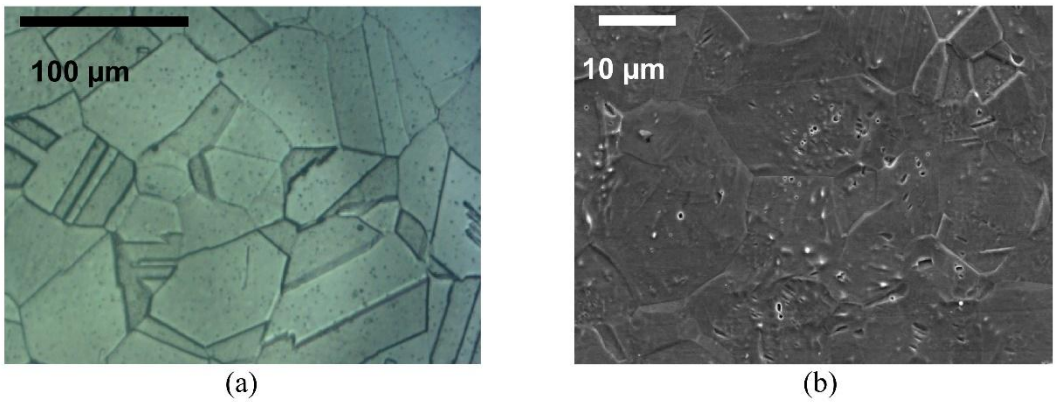

Figure 1: Microstructures of the studied material in the as received state OM (a) and SEM (b).

Fig. 2 presents the XRD patterns of the as-received sample. Within the XRD detection limit, only the peaks from the austenitic phase were identified.

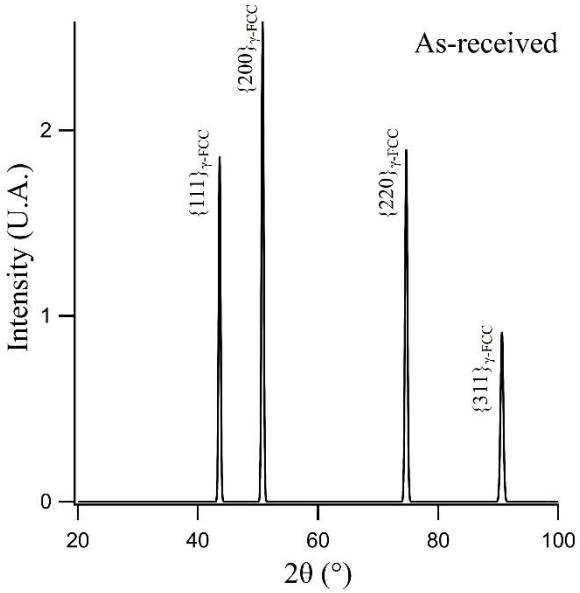

Figure 2: XRD pattern of the as-received sample.

Stacking fault energy (SFE) controls the deformation mechanisms of ASSs. A lower SFE makes dislocation cross-slip more difficult which results in less dislocation mobility and promoting the formation of a larger amount of DIM. The evaluated SFE of the studied steel, adopting the equation (3) suggested by Schramm and Reed [25, 26], is about 50 mJ/m^2:

$$SFE\ (mJ/m^2) = -\ 53 + 6.2(\%Ni) + 0.7(\%Cr) + 3.2(\%Mn) + 9.3(\%Mo) \quad (3)$$

SFE values for the most common austenitic stainless steel series are in the range from 9.2 to 80.7 mJ/m^2 [25, 26]. Therefore, the studied steel displays an intermediate value and as a consequence, cellular dislocation distribution, DIM and deformation bands can be found in the deformed microstructure.

The microstructures of the studied material after 50 % and 75 % cold rolling (Sample A) are presented in Fig. 3. Microstructural analysis using optical microscopy, as shown in Fig. 3, has not allowed differentiation between the different deformation features. The CR of as received samples up to ~50 % thickness reduction, resulted in the formation of a partial typical fibrous structure (containing shear bands (SB)) with some deformed austenite grains (Dγ), as shown in **Fig. 3a**. The microstructure is transformed into fibrous type structure (FS), after 75 % of CR (**Fig. 3b**).

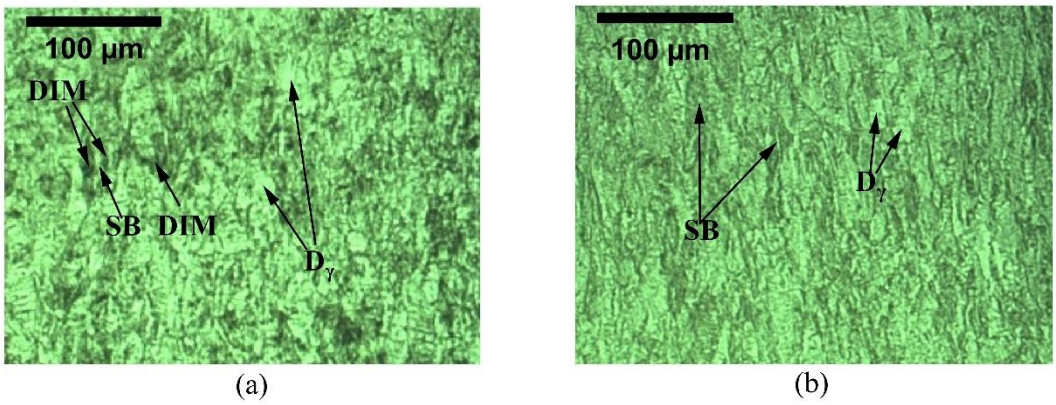

Figure 3: Microstructures of the studied material after 50 % (a) and 75 % (b) cold rolling observed by OM.

X-ray diffraction patterns of 50 % and 75 % cold rolled samples are shown in **Fig. 4 (a)**. As compared with the sample without deformation, new diffraction peaks appear after rolling, indicating the occurrence of the deformation-induced transformation $\gamma \rightarrow \alpha'$ during the CR operation. The absence of the ε-martensite diffraction peaks, which has been mentioned by other researchers [25 - 28], can be explained as follows: the surface of the 50 and 75 % CR samples is the most deformed zone and as consequence, it will contain very small amounts of the ε-martensite due to the ε-martensite → α'-martensite transformation as the deformation is increased. Moreover, the fact that the ε-martensite consists of overlapping stacking faults [26, 28] implies very low intensities, that's why it was not identified by XRD technique.

According to Fig. 4, the increase in thickness reduction from 50 % to 75 % has induced several effects:

(i) An increase in the α'-martensite estimated volume fraction from 55 % to 75 % (Fig. 4b). This may be attributable to the increase in martensite germination sites. As shown by the microstructures presented in Fig. 3, there is an increase of the number of deformation bands which are the main sites of martensite nucleation [4, 9, 10, 17 - 19].

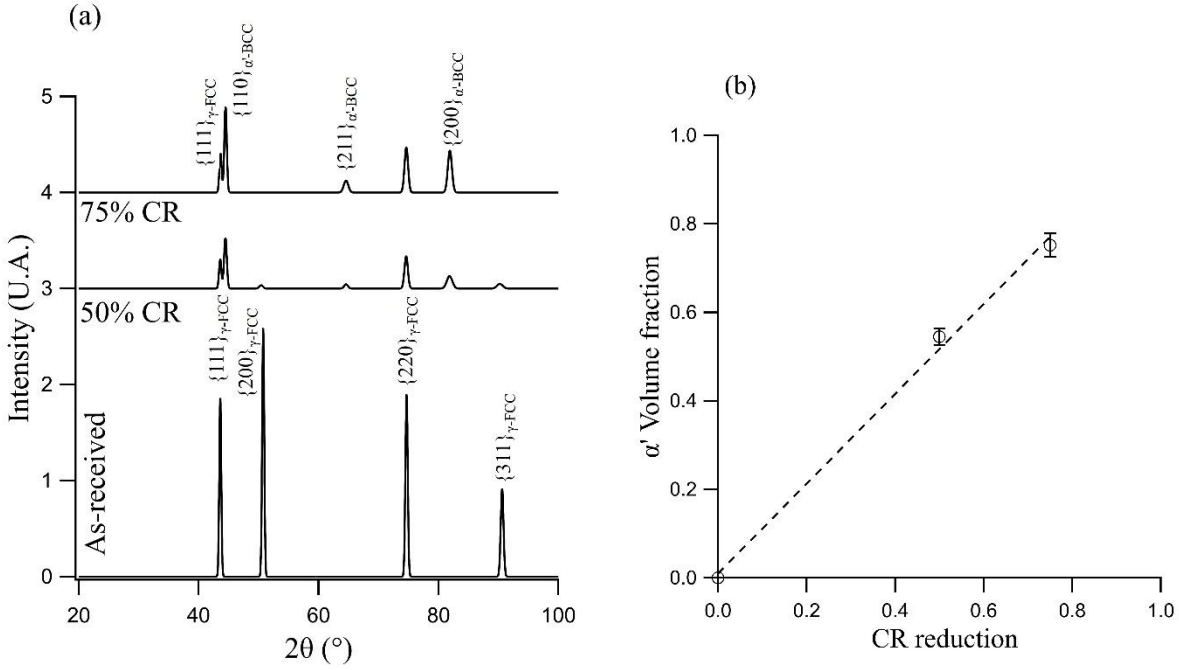

Figure 4: X-ray diffraction patterns of 50 % and 75 % CR samples (a) and evolution of the DIM volume fraction with the CR reduction (b).

(ii) An increase of the Full Width at Half Maximum (FWHM) values of the austenite diffraction peaks (Table 3). This can be attributed to two reasons: (1) the increase of residual stresses in the austenite due to plastic deformation and martensite formation which causes further deformation of the untransformed austenite and (2) the fragmentation of the austenitic grains into small sub-grains by the rearrangement of dislocations in the form of a sub-grain boundary [29].

(iii) A decrease in FWHM values of α'-martensite (Table 3). This effect probably refers to the increased driving force of the martensitic transformation, as the strain ratio is increased, which promotes the formation of coarser martensitic particles.

Table 3. Dependence, on cold rolling ratio, of FWHM values of the austenite main and α'-martensite X-ray reflections.

	Austenite FWHM		**α'-martensite FWHM**	
	{111}	**{220}**	**{110}**	**{211}**
0 %	0.0748	0.1035	-	-
50 %	0.4825	0.7555	0.0566	0.9014
75 %	0.5164	0.8177	0.4310	0.8426

The OM and XRD results after each step of the two-step CR treatment are shown in **Fig.5** and **6**. From these figures, the first cold rolling of 50 % has led to a microstructure constituted of α'-martensite and an untransformed austenite. On the other hand, the volume fraction of the untransformed austenite, estimated from the XRD measurement, is about 45 %.

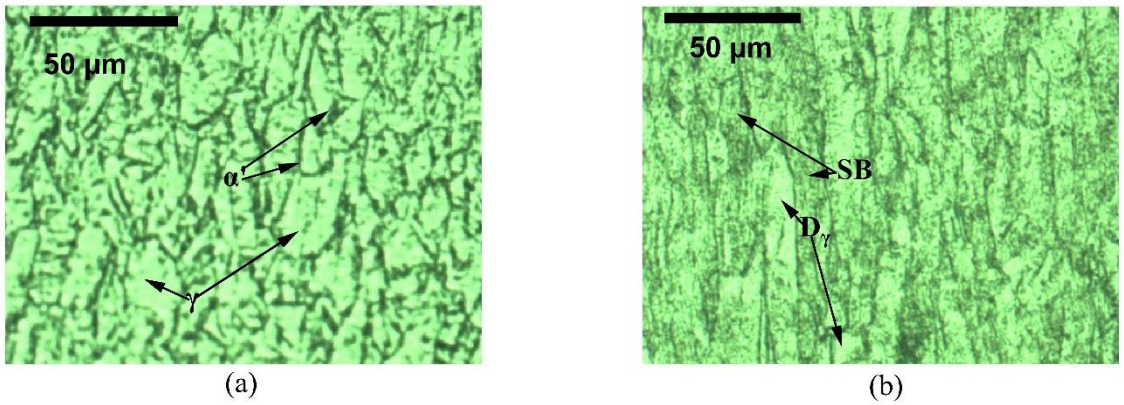

Figure 5: Optical micrographs of samples that were: (a) CR 50 % then annealed 10 min at 810 °C and (b) CR 50 %, treated 10 min at 810 °C then CR 50 %.

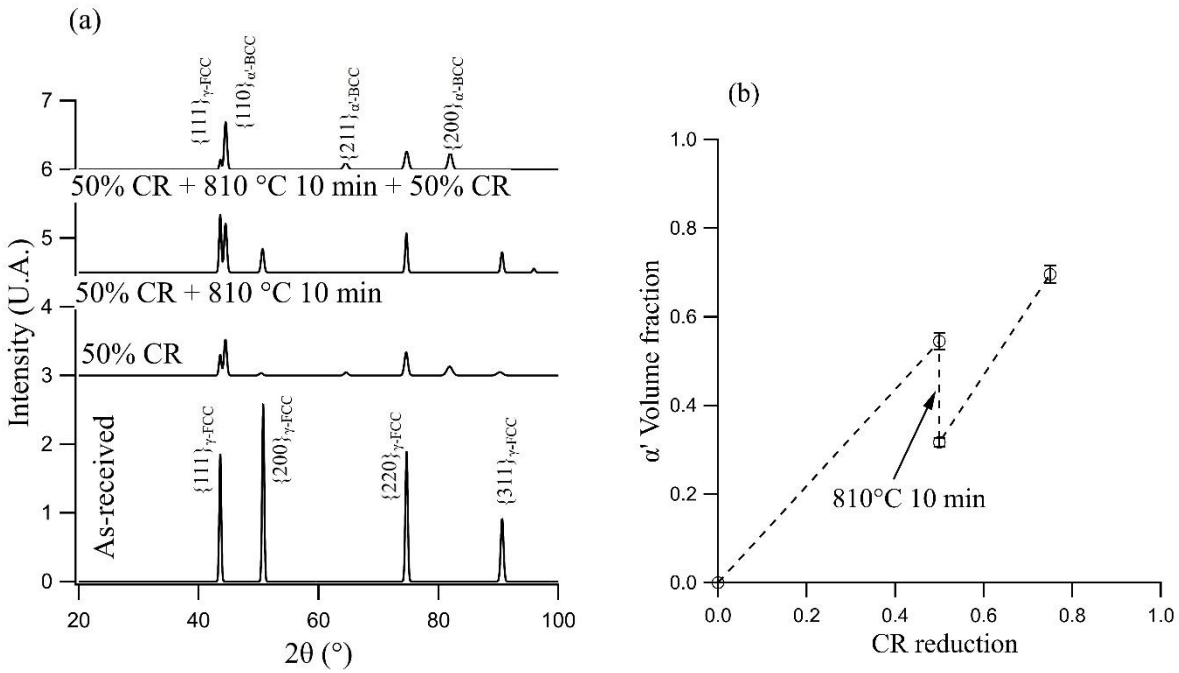

Figure 6: XRD patterns of a sample that was: CR up to 50 %, CR 50 % then annealed 10 min at 810 °C and CR 50 %, treated 10 min at 810 °C then CR 50 %. (a) and corresponding DIM volume fraction evolution (b).

The heat treatment of 10 min at 810 °C has led to a partial reversion of α'-martensite and the recrystallization of the deformed austenite as indicated by a drop in the FWHM values of the austenite diffraction peaks (Table 4).

Table 4. Evolution of the FWHM values of the austenite phase with the thermomechanical process.

	{111}	**{220}**
CR 50 %	0.4818	0.7545
CR50 % + 10 min / 810 °C	0.3165	0.3464

The obtained microstructure after the second CR of 50 % contains 70 % of α'-martensite. Similarly, to sample A, on the microstructure of sample B, only deformed austenite grains (Dγ) and shear bands (SB) can be distinguished.

3.2. Dilatometric results

As it was mentioned above, the deformed microstructures contain cellular dislocation distribution, DIM and deformation bands, consequently, continuous heating allowed the occurrence of recovery, martensite reversion and recrystallization reactions. Furthermore, owing to the different atomic packing factor of austenite and martensite, the reverse transformation $\alpha' \rightarrow \gamma$ occurred while heating can be easily investigated by dilatometric experiments [9, 15, 17, 21, 27, 29-31].

The measured dilatometric curve of sample A, is shown in Fig. 7. This dilatometric behavior has not been reported before. The derivative of the heating segment (the alpha physic curve) indicates the presence of five dilatometric effects (denoted (a) - (e)) appearing in the following order:

- A large split and asymmetric contraction (a) in the temperature range [40 – 400 °C]. The asymmetric shape of this contraction indicates that it may be the result of the overlapping of, at least, two reactions.
- A gradual increase in the apparent thermal expansion coefficient is observed as the temperature is increased up to 400 °C.
- Three separated contractions (b), (d) and (e), having minimums located around 590, 740 and 885 °C, respectively.
- An expansion (c) with a maximum located around 675 °C.

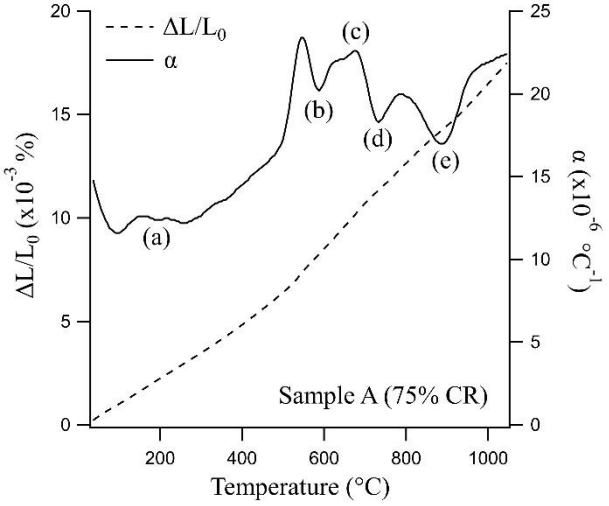

Figure 7: Dilatometric curve, recorded along RD, during continuous heating of sample A.

The dilatometric behavior recorded during the continuous heating of sample B (Fig. 8) is different from the one recorded for material A. In point of fact, one can state the appearance of three dilatometric effects in the following order:

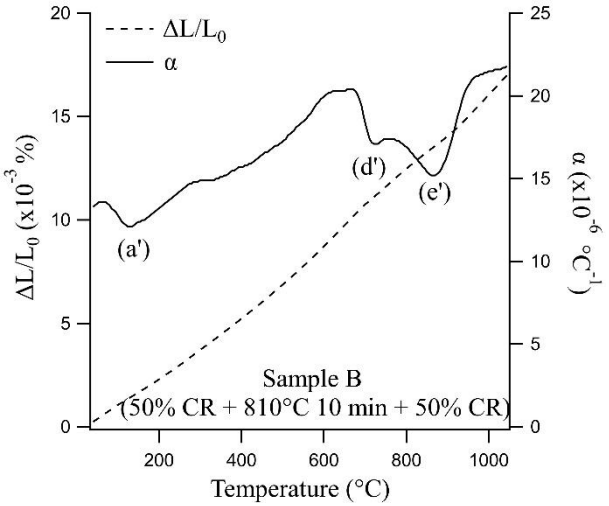

Figure 8: Dilatometric curve, recorded along RD, during continuous heating of sample B.

- A contraction (a') in the temperature range of [60 - 290 °C] is relatively more important than the one recorded for sample A.

- An increase in the values of the coefficient of thermal expansion of approximately $1.35.10^{-5}$ to 2.10^{-5} /°C is observed between 275 and 620 °C.

- A plateau is observed between 620 and 680 °C.

- A significant double contraction ((d') and (e')) in the temperature range of [680 - 1000 °C], with the minimums located around 725 °C and 865 °C, respectively.

The main difference between the two dilatometric curves is the replacement of contraction (b) and expansion (c) by a plateau.

In order to explain the observed dilatometric effects and to check the reverse phase transformation during heating, XRD measurements were carried out on specimens of samples A and B which were previously heated, at a heating rate of 5 °C / min, up to the characteristic temperatures of the different dilatometric effects and then water quenched.

Figure 9a shows the X-ray diffraction patterns of sample A annealed at different temperatures. From the variation of the relative intensities and peak broadening of austenite and martensite phases, the main statements can be summarized as follows:

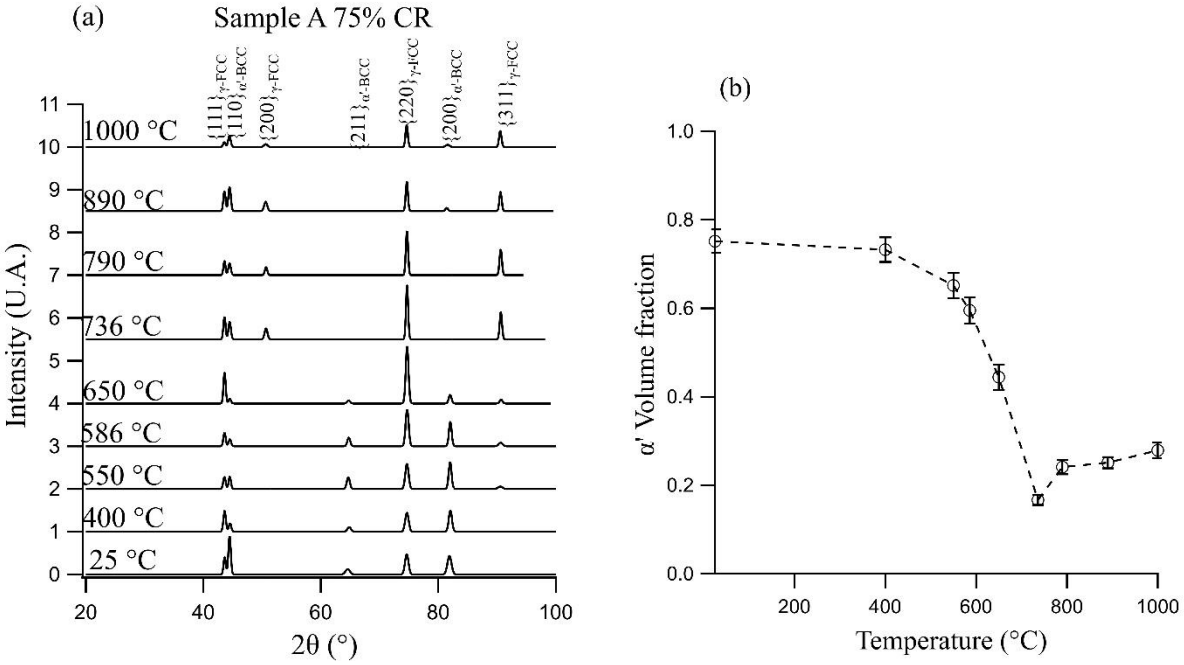

Figure 9: X-ray diffraction patterns of sample A heated at 5 °C/min at different temperatures: from 25 to 1000 °C (a) and the dependence of DIM volume fraction on temperature for sample A (b).

The decrease in the FWHM values of the austenite diffraction peaks as the temperature is increased up to 400 °C (Table 5) is probably due to the reduction of dislocation density during the recovery reaction. The occurrence of this reaction at relatively low temperatures refers to its large driving force (the stored energy) which comes from two sources: (1) the high density of dislocations introduced by the 75 % CR and (2) the stresses induced in the austenite following the formation of DIM (α').

Table 5. Dependence of FWHM values of the austenite main X-ray reflections on temperature.

	{111}	**{220}**
25 °C	0.4974	0.8065

400 °C	0.3983	0.7381

As it has been reported in previous works [17, 18], CR produces the formation of the ε-martensite which can be a transient phase and / or a precursor for the α'-martensite. In contrast to α', the reversion of the ε-martensite takes place at a lower temperature and produces an expansion [17, 18, 30, 31]. Accordingly, the dilatometric anomaly, observed during heating between 25 °C and 400 °C, can be explained by the competition between two reactions: the recovery reaction, as it was mentioned earlier, and the reversion of the ε-martensite.

The gradual increase in the apparent thermal expansion coefficient, observed as the temperature is increased up to 400 °C, can be explained by the ferromagnetic to the paramagnetic transition of martensite [17].

To assess the temperature dependence of α'-martensite reversion, the α'-martensite volume fraction has been calculated (Fig. 9b). The obtained results prove that the anomalous dilatometric effects observed between 550 °C and 1000 °C are, at least, due to reverse transformation ($\alpha' \rightarrow \gamma$).

For several researchers [17, 18, 30, 31], there are two mechanisms of the martensite to austenite reversion; the first one is a without diffusion mechanism (by shear) while the second is a diffusional mechanism. Accordingly, the dilatometric effects (b) and (c) can be explained as follows: when the temperature is increased between 550 and 650 °C, the reversion of the α'-martensite (creating the contraction (b)) is controlled by the shear mechanism and leads to the deformation of the surrounding untransformed austenite. Hence, the expansion (c) production, resulted from the increase in dislocation density, perfectly complies with the findings of an earlier study [27]. For higher temperatures, the diffusion becomes easier and the diffusional reversion takes place and gives the contraction (d). Additionally, from Fig. 10, showing the variation of the microhardness values as a function of temperature, the two contractions (b) and (d) correspond to a significant decrease in microhardness values confirming their attribution to the α'-martensite reversion transformation. An interesting observation, shown in Fig.9 (b), is the increase in DIM content for annealing temperatures above 736 °C. This phenomenon has been reported in several works [33 - 35] and the main explanation that has been given is that cooling after higher annealing temperatures causes the formation of thermally induced martensite. This refers to an increase in the austenite grain size, and / or carbon depletion from the matrix due to the formation of carbides. From Fig.10, the increase in temperature

above 736 °C hasn't led to an increase in the microhardness value, thus, the corresponding increase in α'-martensite content is probably not due to thermally induced martensite (during cooling). A more likely argument for the increase in martensite content for annealing temperatures above 736 °C is the formation of texture in the reversed austenite as was reported in other works [25, 36 - 38].

The authors of [26] have indicated that recrystallization of the ASSs occurs at temperatures higher than the martensite reversion temperature, as a consequence, the last dilatometric effect (e) could be assigned to a recrystallization reaction and texture formation in the deformed austenite. The decrease in the microhardness values after a further increase in temperature (Fig. 10) can be attributed to recrystallization and grain growth of the reverted austenite.

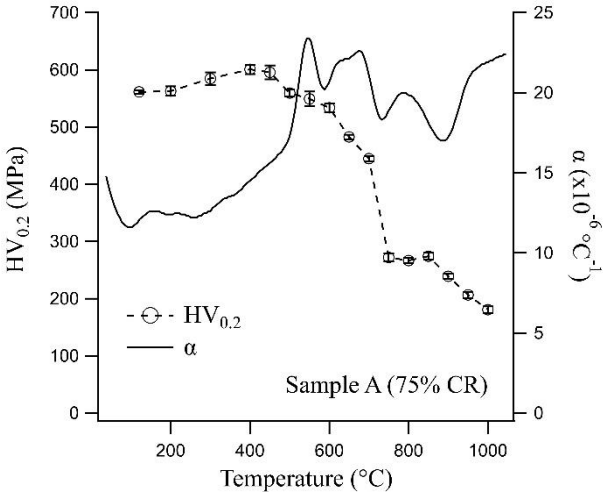

Figure 10: The variation of the microhardness values $HV_{0.2}$ as a function of temperature for sample A.

Based on the aforementioned findings, the sequence of structural changes of sample A, occurring during the continuous annealing, can be summarized as follows:

During heating to 400 °C, the competition between recovery and ε- martensite reversion transformations, led to an asymmetric contraction. The reverse transformation of α'-martensite took place for temperatures above 500 °C and led to a complicated dilatometric anomaly. The occurrence of the athermal reversion of the α'-martensite (for temperatures between 550 and 680 °C) led to two small dilatometric effects: a contraction due to the athermal reversion reaction and a small expansion towing to the austenite deformation resulting from the athermal reversion. Thermal or diffusional reversion of α'-martensite occurs when the temperature was increased up to 780 °C and led to a contraction. Further increase in temperature led to the occurrence of the recrystallization transformation in the deformed austenite resulting in a contraction.

Similarly to sample A, the dilatometric behavior of material B (Fig. 8) can be explained as follows:

(i) The low temperature contraction (a') probably refers to the recovery phenomenon in the deformed austenite.

(ii) The increase in the thermal expansion coefficient values (observed between 275 and 620 °C) can be attributed, at least, to the ferromagnetic to the paramagnetic transition of the α'-martensite.

(iii) The contractions (d') and (e') can be, respectively, attributed to: (1) diffusional reversion of the α'-martensite and (2) the occurrence of the recrystallization reaction in the austenite phase.

To further verify the above scenario of phase transformations, XRD measurements were carried out in the temperature range of 25 - 1000 °C. The obtained results are presented in Fig. 11.

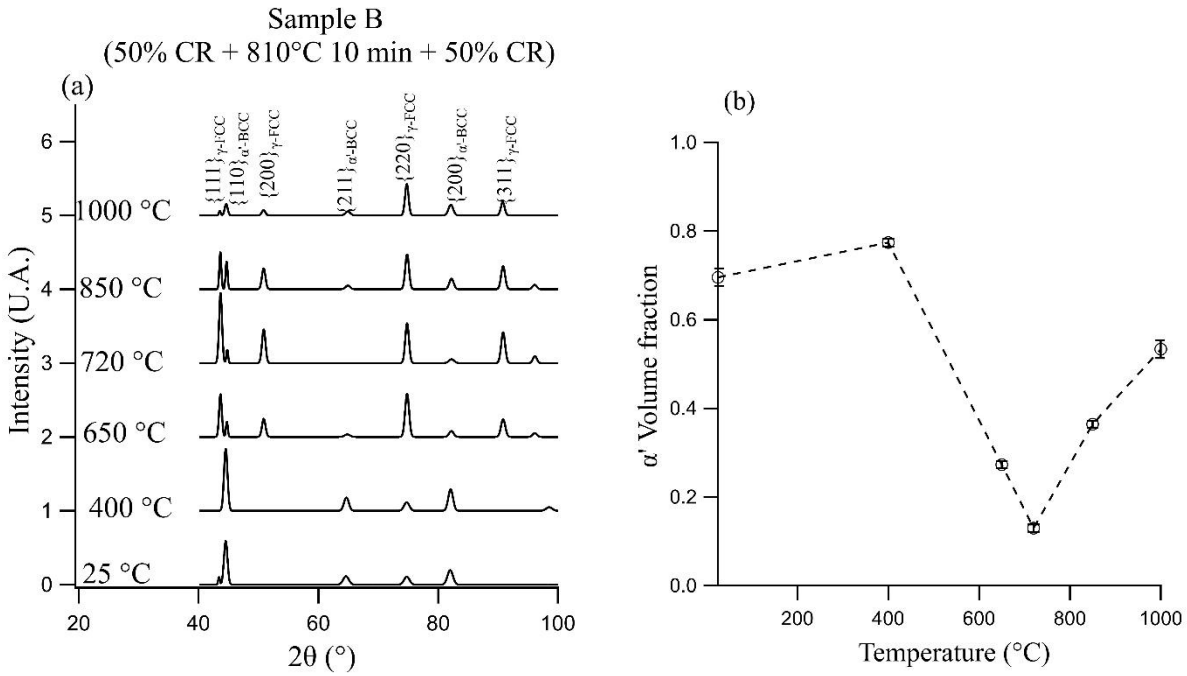

Figure 11: X-ray diffraction patterns of sample B heated at 5 °C/min at different temperatures (a) and the dependence of DIM volume fraction on temperature for sample B (b).

Based on several previous works [6, 17, 27, 32- 35] **Fig.11b** and **12 which, respectively,** illustrate both the evolution of α'-martensite volume fraction and microhardness as a function of temperature. The occurrence of the different dilatometric effects can be explained as follows:

- During the first stage of continuous annealing, the occurrence of the recovery reaction in the untransformed austenite produces the contraction (a'). Further increase in temperatures up to 620 °C leads to

an increase in the coefficient of thermal expansion values due to the ferromagnetic to paramagnetic transformation of the α'-martensite. The appearance of a plateau between 620 – 680 °C can be explained by the overlapping of several reactions: (i) the reversion of ε-martensite, which leads to an expansion and (ii) the athermal reversion of α'-martensite which produces, as it's discussed above, a contraction followed by an expansion.

-The continuous annealing for temperatures above 670 °C leads firstly to the thermal reversion of α'-martensite and then to the recrystallization reaction.

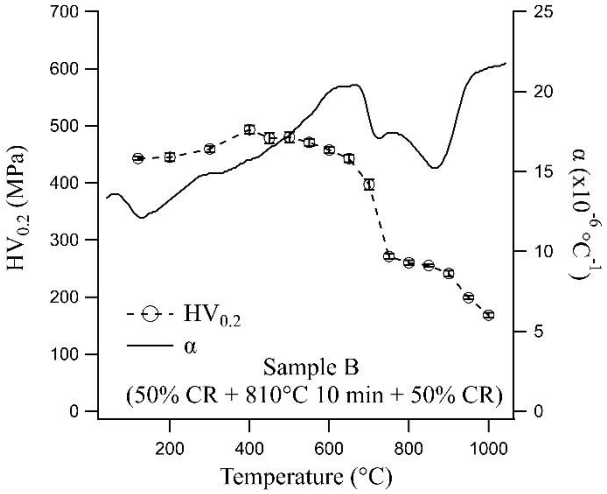

Figure 12: The variation of the microhardness values as a function of temperature for sample B.

As it was demonstrated above, the microstructure obtained after two-step CR (sample B) contains a lower content of α'-martensite and less deformed austenite grains. Consequently, the plateau observed between 620 and 680 °C, which was related to an overlap between the ε-martensite reversion and the α'-martensite athermal reversion, can be explained by the relatively higher reversion temperature of ε-martensite. This can be understood by the fact that lower strain promotes coarser and more stable ε-martensite.

4. Conclusions:

The sequence of structural changes produced in two deformed microstructures elaborated by a multi-pass CR and a two-step CR to a 75 % thickness reduction, were followed by dilatometry. The two materials showed different dilatometric behaviors. XRD and microhardness measurements were used underlying the observed dilatometric behavior. The main results can be summarized as follows:

The material subjected to multi-pass unidirectional CR to a 75 % thickness reduction, showed an unusual dilatometric behavior. During the first stage of heating (up to 400 °C), the competition between the recovery

and the ε-martensite reversion led to an asymmetric contraction. When the temperature was increased between 550 and 780 °C, the reverse transformation of α'-martensite took place and led to a complicated dilatometric anomaly. Firstly, the occurrence of the athermal reversion of α'-martensite led to two small dilatometric effects: a contraction due to the reversion reaction and a small expansion towing to the austenite deformation deriving from the athermal reversion. Thermal reversion of α'-martensite occurred at high temperatures and led to a contraction. Further increase in temperatures led to the occurrence of the recrystallization transformation.

The material subjected to two-step CR showed a quite usual dilatometric behavior which was explained by the occurrence of several reactions in the following order:

- During the first stage of heating, the occurrence of recovery reaction produced a contraction.
- The increase in temperature up to 620 °C led to an increase in the thermal expansion coefficient values due to the ferromagnetic to paramagnetic transformation of α'-martensite. The appearance of a small plateau between 620 - 680 °C was supposed to be due to the overlap of several reactions: (i) the ε-martensite reversion and (iii) the athermal reversion of α'-martensite.
- Further increase in temperature above 680 °C led first to the thermal reversion of α'-martensite and then the recrystallization transformation.

5. References:

[1] T.H. Courtney, Mechanical Behavior of Materials, McGraw-Hill, New York (2000).

[2] M.A Meyers, and K.K. Chawla, Mechanical Behavior of Materials, second Edition, Cambridge University Press, Cambridge (2008).

[3] R.W. Hertzberg, R.P. Vinci, and J.L. Hertzberg, Deformation and Fracture Mechanics of Engineering Materials, Fifth edition, John Wiley & Sons, Inc., New York (2012).

[4] S. K. Ghosh, Shikhar Jha, P. Mallick, and P. P. Chattopadhyay, Influence of Mechanical Deformation and Annealing on Kinetics of Martensite in a Stainless Steel, Mater. Manuf. Process, 28 (2013) 249 – 255.

[5] D. Chatterjee, Effect of repeated warm rolling cold rolling and annealing on the microstructure and mechanical properties of AISI 301LN grade austenitic stainless steel, Mater. Today, 46 (2021) 10604–10611.

[6] I. Shakhova, V. Dudko, A. Belyakov, K. Tsuzaki, R. Kaibyshev, Effect of large strain cold rolling and subsequent annealing on microstructure and mechanical properties of an austenitic stainless steel, Mater. Sci. Eng. A, 545 (2012) 176– 186.

[7] C. Celada-Casero, B.M. Huang, J.-R. Yang, D. San-Martin, Microstructural mechanisms controlling the mechanical behaviour of ultrafine grained martensite/austenite microstructures in a metastable stainless steel, Mater. Des. 181 (2019) 107922.

[8] K. Hao, M. Gao, R. Wu, Cold rolling performance for austenitic stainless steel with equilibrium and non-equilibrium microstructures, J. Mater.Res. Technol. 9(1) (2020) 124–132.

[9] Y. He, J. Zhang, Y. Wang, Y. Wang, T. Wang, The expansion behavior caused by deformation-induced martensite to austenite transformation in heavily cold-rolled metastable austenitic stainless steel, Mater. Sci. Eng. A 739 (2019) 343–347.

[10] A Hedayati, A. Najafizadeh, A. Kermanpur, F. Forouzan, The effect of cold rolling regime on microstructure and mechanical properties of AISI 304L stainless steel, J. Mater. Process. Technol., 210 (2010) 1017–1022.

[11] A. Amininejad, R. Jamaati, S. J. Hosseinipour, Achieving superior strength and high ductility in AISI 304 austenitic stainless steel via asymmetric cold rolling, Mater. Sci. Eng. A 767 (2019) 138433.

[12] C. Zheng, C. Liu, M. Ren, H. Jiang, L. Li, Microstructure and mechanical behavior of an AISI 304 austenitic stainless steel prepared by cold- or cryogenic-rolling and annealing, Mater. Sci. Eng. A, 724 (2018) 260–268.

[13] W. Mao, S. Gao, Y. Bai, M. Park, A. Shibata, N. Tsuji, Effective grain size refinement of an Fe-24Ni-0.3C metastable austenitic steel by a modified two-step cold rolling and annealing process utilizing the deformation-induced martensitic transformation and its reverse transformation, J. Mater. Res. Technol., 17 (2022) 2690 – 2700.

[14] J.X.Huang, X.N. Ye , Z. Xu, Effect of Cold Rolling on Microstructure and Mechanical Properties of AISI 301LN Metastable Austenitic Stainless Steels, J. Iron Steel Res. Int., 19(10) (2012) 59 – 63.

[15] M.Moallemi, A. Zarei-Hanzaki, H.S.Baghbadorani, Evolution of microstructure and mechanical properties in a cold deformed nitrogen bearing TRIP-assisted duplex stainless steel after reversion annealing, Mater. Sci. Eng. A 683 (2017) 83 – 89

[16] W. He, F. Li, H. Zhang, H. Chena, H. Guo, The influence of cold rolling deformation on tensile properties and microstructures of Mn18Cr18 N austenitic stainless steel, Mater. Sci. Eng. A, 764 (2019) 138245.

[17] P. Dastur, A. Zarei-hanzaki, R. Rahimi, M. Moallemi, V. Klemm, B.C. DE Cooman, and J. Mola, Martensite Reversion Duality Behavior in a Cold-Rolled High Mn Transformation-Induced Plasticity Steel, Metall. Mater. Trans. A, 50 (2019) 4550 – 4560.

[18] Y Tian, O. I. Gorbatov, A. Borgenstam, A. V. Ruban, and P. Hedström, Deformation Microstructure and Deformation-Induced Martensite in Austenitic Fe-Cr-Ni Alloys Depending on Stacking Fault Energy, Metall. Mater. Trans. A, 48 (2017)1–7.

[19] A. K. De, D. C. Murdock, M. C. Mataya, J. G. Speer, D. K. Matlock, Quantitative measurement of deformation-induced martensite in 304 stainless steel by X-ray diffraction, Scr. Mater., 50 (2004) 1445–1449.

[20] N. H. Moser, T. S. Gross, and Y. P. Korkolis, Martensite Formation in Conventional and Isothermal Tension of 304 Austenitic Stainless Steel Measured by X-ray Diffraction, Metall. Mater. Trans. A 45 (2014) 4891–4896.

[21] J. Mola, D. Chae, and B. C. De Cooman, Dilatometric Analysis of Anisotropic Dimensional Changes in a 16 Pct Cr Stainless Steel with a Planar Banded Structure, Metall. Mater. Trans. A, 41(2010) 1429–1440.

[22] J.T. Bonarski, M. Wróbel, K. Pawlik, Evolution of Microstructure in Rolled Mg-Based Alloy. Textural Aspect, Mater. Sci. Technol., 16 (2000) 657–662.

[23] N. Iskounen, P.A. Dubos, J. Fajoui, M. Coret, M.J. Moya, B. Girault, N. Barrier, N. Bruzy, E. Hug, D. Gloaguen, Experimental investigation of allotropic transformation of cobalt: influence of 1 temperature cycle, mechanical loading and starting microstructure, Metall. Mater. Trans. A 52 (4) (2021) 1477 – 1491.

[24] P.A. Dubos, J. Fajoui, N. Iskounen, M. Coret, S. Kabra, J. Kelleher, B. Girault, D. Gloaguen, Temperature effect on strain-induced phase transformation of cobalt, Mater. Lett. 281 (2020) 128812.

[25] G. Fargas, A. Zapata, J. J. Roa, I.Sapezanskaia and A. Mateo, Correlation Between Microstructure and Mechanical Properties Before and After Reversion Of Metastable Austenitic Stainless Steels, Metall. Mater. Trans. A 46A, (2015) 5697 – 5707.

[26] J.X. Huang, X.N. Ye and Z. Xu, Effect of cold rolling on microstructure and mechanical properties of AISI 301LN metastable austenitic stainless steels, J. Iron Steel Res. Int. Vol. 19 (10) (2012) 59 – 63.

[27] A. F. Padilha, R. L. Plaut and P. R. Rios, ISIJ International, Vol. 43 (2003), No. 2, pp. 135–143.

[28] J. Huang, X. Ye, J. Gu, X. Chen and Z. Xu, Mater. Sci. Eng. A, 2012, vol. 532, pp. 190–95.

[29] G.-S. Sun, J. Hu, B. Zhang, L.-X. Du, The significant role of heating rate on reverse transformation and coordinated straining behavior in a cold-rolled austenitic stainless steel, Mater. Sci. Eng. A 732 (2018) 350 – 358.

[30] G. Cios, T. Tokarski, A. Zywczak, R. Dziurka, M. Stepien´, Ł. Gondek, M. Marciszko, B. Pawłowski, K. wieczerzak, and P. Bała, The Investigation of Strain-Induced Martensite Reverse Transformation in AISI 304 Austenitic Stainless Steel, Metall. Mater. Trans. A 48 (2017)4999–5008.

[31] T.F.A. Santos and M.S. Andrade, Dilatometric evaluation of strain-induced martensite reversion in AISI 304 austenitic stainless steel, Revista Matéria, 13 (4) (2008) 587 – 596.

[32] D.L. Johannsen, A. Kyrolainen and P.J. Ferreira, Influence of Annealing Treatment on the Formation of Nano/Submicron Grain Size AISI 301 Austenitic Stainless Steels, Metall. Mater. Trans. A Vol. 37A (2006) 2325–2338.

[33] R. Ueji, N. Tsuji, Y. Minamino and Y. Koizumi, Ultragrain refinement of plain low carbon steel by cold-rolling and annealing of martensite, Acta Mater., Vol. 50 (2002) 4177 – 89.

[34] Y.K. Lee, C.H. Shi, D.S. Leem, J.Y. Choi, W. Jin and C.S. Choi, Reverse transformation mechanism of martensite to austenite and amount of retained austenite after reverse transformation in Fe-3Si-13Cr-7Ni (wt-%) martensitic stainless steel**,** Mater. Sci. Technol., Vol. 19 2(003) 393 – 98.

[35] B. Ravi Kumar, B. Mahato, N. R. Bandyopadhyay, D. K. Bhattacharya, Influence of strain-induced phase transformation on the surface crystallographic texture in cold-rolled and aged austenitic stainless steel, Metall. Mater. Trans. A 36 (2005) 3165 – 3174.

[36] A. Poulon, S. Brochet, J.B. Vogt, J.C. Glez, J.D. Mithieux, Fine grained austenitic stainless steels: the role of strain induced α' martensite and the reversion mechanism limitations, ISIJ Int., 49 (2009) 293–301.

[37] B. Ravi Kumar, A.K. Singh, B. Mahato, P.K. De, N.R. Bandyopadhyay, D.K. Bhattacharya, Deformation-induced transformation textures in metastable austenitic stainless steel, Mater. Sci. Eng. A 429 (2006) 205–211.

[38] B. Ravi Kumar, A.K. Singh, S. Das, D.K. Bhattacharya, Cold rolling 304 stainless steel, Mater. Sci. Eng. A 364 (2004) 132–139.